THE JOURNAL OF PHYSICAL CHEMISTRY C

Article

pubs.acs.org/JPCC

A Postsynthetic Modification of II–VI Semiconductor Nanoparticles to Create Tb^{3+} and Eu^{3+} Luminophores

Prasun Mukherjee,[†,§] Robin F. Sloan,[†] Chad M. Shade,[†] David H. Waldeck,*[,†] and Stéphane Petoud*[,†,‡]

[†]Department of Chemistry, University of Pittsburgh, Pittsburgh, Pennsylvania 15260, United States

[‡]Centre de Biophysique Moléculaire, CNRS UPR 4301, rue Charles Sadron, 45071 Orléans, France

Supporting Information

ABSTRACT: We describe a novel method for creating luminescent lanthanide-containing nanoparticles in which the lanthanide cations are sensitized by the semiconductor nanoparticle's electronic excitation. In contrast to previous strategies, this new approach creates such materials by addition of external salt to a solution of fully formed nanoparticles. We demonstrate this postsynthetic modification for the lanthanide luminescence sensitization of two visible emitting lanthanides (Ln), Tb^{3+} and Eu^{3+} ions, through ZnS nanoparticles in which the cations were added postsynthetically as external $Ln(NO_3)_3{\cdot}xH_2O$ salt to solutions of ZnS nanoparticles. The postsynthetically treated ZnS nanoparticle systems display Tb^{3+} and Eu^{3+} luminescence intensities that are comparable to those of doped Zn(Ln)S nanoparticles, which we reported previously (*J. Phys. Chem. A*, **2011**, *115*, 4031–4041). A comparison with the synthetically doped systems is used to contrast the spatial distribution of the lanthanide ions, bulk versus surface localized. The postsynthetic strategy described in this work is fundamentally different from the synthetic incorporation (doping) approach and offers a rapid and less synthetically demanding protocol for Tb^{3+}:ZnS and Eu^{3+}:ZnS luminophores, thereby facilitating their use in a broad range of applications.

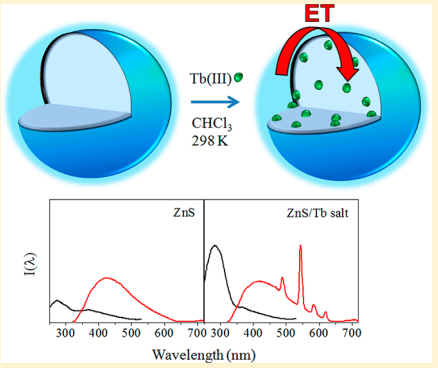

INTRODUCTION

Because of their unique luminescence properties,[1−10] lanthanide cations (Ln^{3+}) are of considerable interest for a broad range of applications; including telecommunications, energy conversion, bioanalysis, and biological imaging applications. Their 4f–4f transitions appear as sharp emission bands that are distributed over the visible and near-IR spectral regions, and their wavelength maxima do not shift upon change of external conditions, such as temperature, pH, or biological environment. Because of their minimal overlap and "fingerprint" character,[9] these luminescence bands are attractive candidates for use in multiplex assays. Because the lanthanide luminescence is long-lived (microsecond to millisecond time domain), time-gated luminescence measurements offer a method to discriminate the emission from nanosecond-lived background species, thus providing an improved signal-to-noise ratio and more sensitive detection. Unlike organic fluorophores, lanthanide luminescence is highly resistant to photobleaching, thereby offering promise for imaging applications.[11]

To exploit Ln^{3+} luminescence in applications, challenges posed by their small oscillator strength and nonradiative relaxation pathways[7] must be overcome. Because of the electric-dipole forbidden nature of the f–f transitions, the molar extinction coefficient of the Ln^{3+} ions are typically extremely small, $\leq 10\ M^{-1}cm^{-1}$.[12−14] To circumvent this limitation and more efficiently excite the lanthanide ions, workers use organic chromophores and/or semiconductor materials as sensitizers that absorb incident photons and transfer the excitation energy nonradiatively to excite the Ln^{3+} ions.[15,16] This indirect excitation of Ln^{3+} ions leads to the same well-defined and long-lived luminescence emission.[2,17−29] Doping of Ln^{3+} ions into an inorganic nanoparticle antenna provides an excellent strategy for both sensitizing the Ln^{3+} emission and increasing its quantum yield by protecting it from high frequency vibrational overtones of −OH, −NH, and −CH stretches, which can strongly quench the luminescence.[30,31] The superior promise of inorganic materials over organic chromophores as antennae derives from this feature. While the benefits of increasing the excitation efficiency and decreasing the nonradiative rates are well appreciated, the advantage of using a high number density of lanthanide ions is less well appreciated. Because detection sensitivity in an application depends directly on the number of photons emitted, using polymetallic lanthanide molecules and materials is a promising strategy for maximizing the number of photons per unit volume.[32−34] In contrast to organic dyes, the luminescence of Tb^{3+}- and Eu^{3+}-doped ZnS nanoparticles exhibit little self-quenching of the Ln^{3+} emission, thereby supporting the strategy of creating materials with a high density of Ln^{3+} ions. For these three reasons, inorganic nanoparticle hosts represent a very promising strategy for improving the efficiency of lanthanide ion luminescence.

Some previous studies have discussed the external addition of metal ions into nanoparticles from salt solution.[35−41] For

Received: May 20, 2013
Published: June 4, 2013

   dx.doi.org/10.1021/jp404947x | *J. Phys. Chem. C* 2013, 117, 14451–14460

example, Alivisatos and co-workers[35] showed that it is possible to produce Ag_2Se nanoparticles by adding Ag^+ ions to a solution of CdSe nanoparticles, and Banin and co-workers[36] have demonstrated the doping of InAs nanoparticles with Cu^{2+}, Ag^+, and Au^{3+} through cation exchange. Murphy and co-workers[37] compared the luminescence properties of Mn^{2+}-doped ZnS nanoparticles with those for which the Mn^{2+} ions were added externally (post nanoparticle synthesis) and found that the luminescence was different. Cation exchange reactions in lanthanide fluoride nanoparticles were first reported by van Veggel and co-workers;[38] however, the host does not act as an antenna in this case. Chen and co-workers[39] have added Tb^{3+} ions externally (postsynthesis) to ZnS nanoparticles in AOT [sodium bis(2-ethylhexyl)sulfosuccinate] reverse micelles and have observed enhanced Tb^{3+} emission; however, their study considers Tb^{3+} ions located on or near the surface of the nanoparticles.[35,38,40,41] In contrast to previous work, our current study compares the photophysical properties of the postsynthetically treated ZnS nanoparticles with those that have Ln^{3+} synthetically incorporated (doped). Sensitization of Tb^{3+} and Eu^{3+} luminescence is analyzed by studying the evolution of the ZnS nanoparticle spectra as Tb^{3+} or Eu^{3+} nitrate salts are added externally to their solutions, which are denoted as ZnS/Ln salt (where the slash indicates a postsynthesis Ln^{3+} salt addition), and by comparing those spectra to the synthetically incorporated Zn(Ln)S systems (the use of parentheses indicates that Ln^{3+} was added during the synthesis of the nanoparticle). The generality of this approach is illustrated by performing the same postsynthetic salt addition strategy to commercially purchased CdS nanoparticles. Finally, the asymmetry ratio and luminescence lifetime of Eu^{3+} cations are used to assess the relative contributions of core and surface localized Eu^{3+} ions.

The postsynthetically treated nanoparticles present a major advantage over the corresponding synthetically incorporated (doped) counterpart. For example, it is possible to synthesize Tb^{3+} and/or Eu^{3+} incorporated nanoparticles starting from one batch of undoped nanoparticles, whereas preparation of the corresponding doped systems requires two separate syntheses. Thus the novel postsynthetic protocol described in the present work reduces the synthetic effort, loss of yield, and other risks significantly. This advantage allows the synthesis of large amounts of luminescent-based materials when the synthesis of lanthanide-based molecular complexes often requires multistep reactions which can require "man-months" of effort.

SENSITIZING Ln^{3+} LUMINESCENCE WITH II–VI SEMICONDUCTOR NANOPARTICLES

General Characterization. High-resolution transmission electron microscopy (HRTEM) images were obtained using a JEOL-2100 CF instrument operating between 120 kV and 200 kV. A TEM image and the corresponding EDS data for Zn(Tb)S nanoparticles are shown in Figure 1. The EDS data were collected with a micrometer scale spot size and demonstrate the presence of terbium. Various other researchers have also presented experimental observations on doping nanosized ZnS materials with Tb^{3+}[39,42] and Eu^{3+}[43−51] cations. The size distribution of the Zn(Tb)S nanoparticles were calculated using the Image J software and found to be 3.7 ± 0.7 nm in average diameter.

Absorption spectra of ZnS nanoparticles show a band centered around 295 nm (see Figure S1 in the Supporting Information). A simple estimation for the size of the nanoparticle based on the method proposed by Brus[52] gives a value of 3.3 nm in diameter and is consistent with the TEM measurement. The dependence of the exciton band position on ZnS nanoparticle growth time was shown in our previous work[31] and by Peng and co-workers.[53]

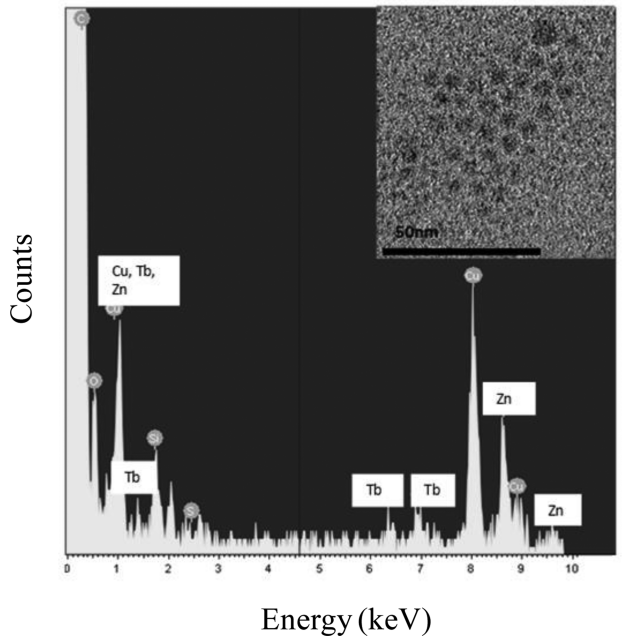

Figure 1. The upper right panel shows an HRTEM image of Zn(Tb)S nanoparticles. An energy dispersive X-ray spectrum (EDS) of doped ZnS that labels the metal peaks is shown. Note that Cu most likely comes from the mounting assembly.

Luminescence Spectra for ZnS Nanoparticle Tb (or Eu) Salt Solutions. Figure 2 presents the steady-state excitation and emission spectra of ZnS/Tb salt, ZnS/Eu salt, and ZnS solutions. Under λ_{ex} = 300 nm excitation, solutions of ZnS nanoparticles show a broad emission band (panels b and d, black) with an apparent maximum at ∼420 nm, which is qualitatively consistent with previous work and is assigned to emission arising from various defect states of the nanoparticles.[31] Panels a and c (black curve) show the ZnS excitation spectra at two different emission wavelengths.

ZnS/Tb Salt (Strategy I, 0.1% Water, See Materials and Methods Section). Upon addition of Tb^{3+} nitrate salt to ZnS nanoparticle solutions, prominent sharp Tb^{3+} luminescence bands appear with well-defined maxima located at ∼490 nm ($^5D_4 \rightarrow {}^7F_6$), ∼545 nm ($^5D_4 \rightarrow {}^7F_5$), ∼585 nm ($^5D_4 \rightarrow {}^7F_4$), and ∼620 nm ($^5D_4 \rightarrow {}^7F_3$) (Figure 2, panel b). The Tb^{3+} emission of the ZnS/Tb salt is similar in intensity to the synthetically incorporated Zn(Tb)S system[31] (see Table 1). By monitoring the sharp emission band centered at ∼545 nm (Tb^{3+} emission) and scanning the excitation wavelength, a broad excitation profile that resembles that of the ZnS excitation spectrum is evident (Figure 2, panel a); however, the band at ∼285 nm is strongly enhanced for the ZnS/Tb salt solution, which implies that it is more efficient in sensitizing the Tb^{3+} emission. In order to evaluate the stability of the lanthanide containing nanoparticles, corresponding spectra were acquired over many days and weeks; even in samples that are ∼2.5 months old, no degradation of the lanthanide centered luminescence is evident. These data indicate that the sensitization of the Tb^{3+} luminescence operates through the electronic excitation of

dx.doi.org/10.1021/jp404947x | J. Phys. Chem. C 2013, 117, 14451−14460

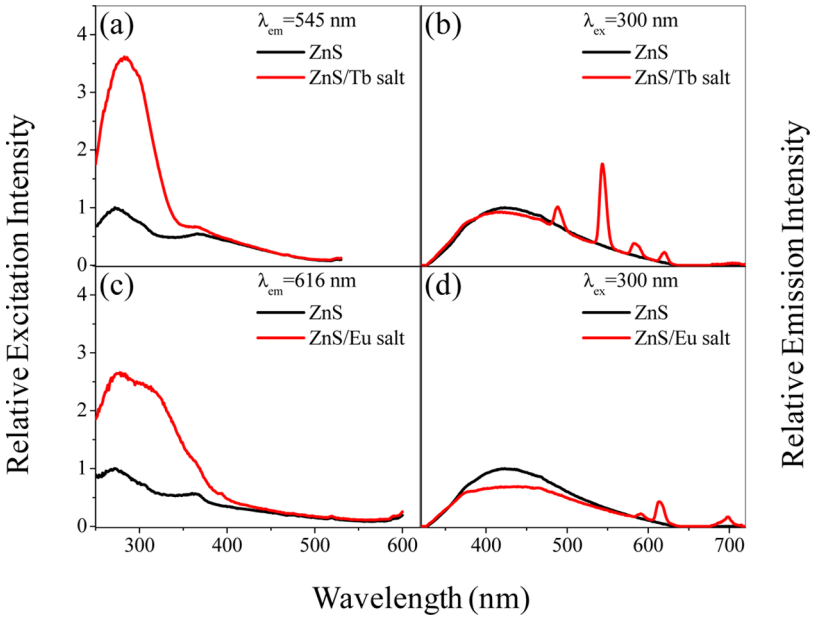

Figure 2. Representative steady-state excitation and emission spectra of ZnS/Tb salt and ZnS/Eu salt solutions are shown and compared to those for ZnS solutions. The nanoparticles were dissolved in chloroform: for the corresponding lanthanide salts, 0.1% water (v/v) was added to the nanoparticle containing chloroform solution. In each panel, the ZnS nanoparticle's emission (black curve) is normalized to unity at the maximum signal intensity and the ZnS/Tb (or Eu) salt spectra (red curve) are shown with respect to it by scaling to the same optical density at the excitation wavelength. Figure S2 in the Supporting Information presents the subtracted excitation spectra.

Table 1. Comparison of Quantum Yields in Different Systems Studied[a]

chloroform solutions	relative Φ_F (Ln^{3+})
Zn(Tb)S	1
Zn(Tb)S[b]	0.93 ± 0.03
ZnS/Tb salt[b]	1.2 ± 0.2
Zn(Tb)S/Tb salt[b]	2.5 ± 0.3
Zn(Eu)S	1
Zn(Eu)S[b]	0.77 ± 0.05
ZnS/Eu salt[b]	0.9 ± 0.2
Zn(Eu)S/Eu salt[b]	1.3 ± 0.2

[a]All values were calculated relative to the value found for the synthetically incorporated Zn(Ln)S system, which was set to unity. All of the solution spectra were adjusted to have an absorbance of 0.2 at 300 nm. [b]Solutions include 0.1% water.

the ZnS nanoparticles in the 285 nm region; the ZnS nanoparticle acts as an antenna.

ZnS/Eu Salt (Strategy I, 0.1% Water, See Materials and Methods Section). External addition of Eu^{3+} ions to a ZnS nanoparticle solution generates Eu^{3+} luminescence bands, which appear at ~590 nm ($^5D_0 \rightarrow {}^7F_1$), ~616 nm ($^5D_0 \rightarrow {}^7F_2$), and ~700 nm ($^5D_0 \rightarrow {}^7F_4$) (Figure 2, panel d). The ZnS/Eu salt system displays a luminescence efficiency that is similar to the synthetically incorporated Zn(Eu)S system (see Table 1). Monitoring the sharp emission signal at 616 nm (Eu^{3+} emission) and scanning the excitation wavelength generates a broad excitation profile that closely resembles that of the ZnS excitation spectrum; however, the band near 300 nm is enhanced over that for the pure ZnS. These data show that the ZnS nanoparticle absorbance sensitizes the Eu^{3+} luminescence (Figure 2, panel c), similar to the situation observed for the ZnS/Tb salt system described above.

ZnS/Eu Salt (Strategy II; No Water, See Materials and Methods Section). Figure 3a compares the steady-state

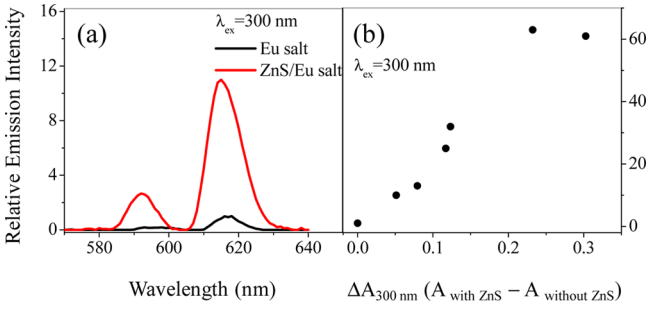

Figure 3. Representative steady-state emission spectra of Eu^{3+} containing systems with and without ZnS nanoparticles are shown in panel a. The experiments were performed by dissolving the salt in chloroform (see Materials and Methods section). Panel b shows a plot of how the $^5D_0 \rightarrow {}^7F_2$ Eu^{3+} luminescence band intensity increases upon addition of ZnS nanoparticles to a ~50 μM overall concentration of $Eu(NO_3)_3$ solution in chloroform (see text for additional details). The relative intensity values are scaled with respect to the corresponding intensity value without the ZnS nanoparticles, which is normalized to unity at the maximum intensity.

emission spectra of Eu^{3+} luminescence bands in a chloroform solution of $Eu(NO_3)_3$ with that for a ZnS/Eu salt solution, after subtraction of the intrinsic ZnS nanoparticle emission. The two solutions have the same concentration of Eu ions, and the spectra are scaled to unity for the peak emission of the $Eu(NO_3)_3$ solutions in order to simplify the comparisons. These data demonstrate that the solutions containing ZnS nanoparticles generate ~10 times more intensity for the Eu^{3+} luminescence.[54] To better quantify the increase in Eu^{3+} luminescence that results from the ZnS nanoparticle's antenna effect, control experiments were performed in which the $Eu(NO_3)_3$ was dissolved in chloroform containing TOP/TOPO/octadecene/tetracosane/0.1% water (the amount of these compounds were adjusted to closely mimic the synthetic

dx.doi.org/10.1021/jp404947x | J. Phys. Chem. C 2013, 117, 14451−14460

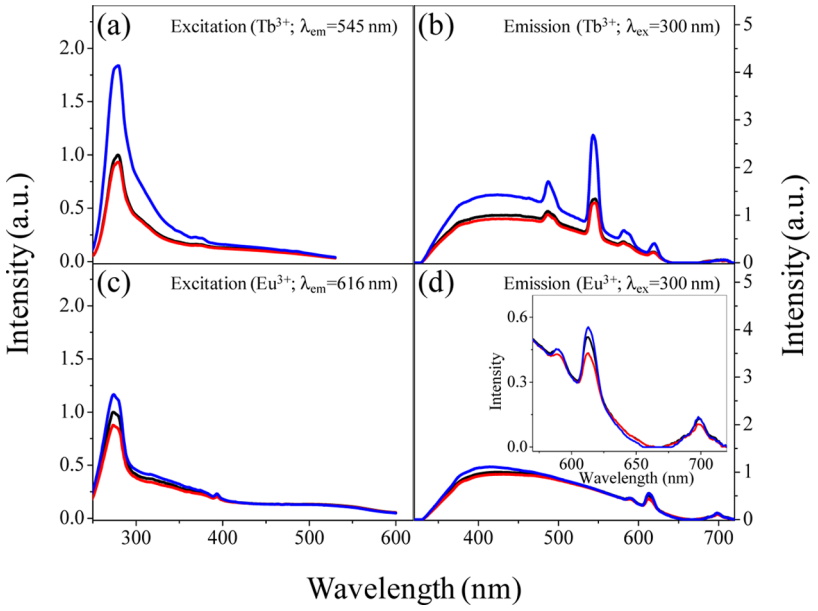

Figure 4. Representative steady-state excitation and emission spectra are shown for the Zn(Tb)S and Zn(Eu)S nanoparticle solutions in chloroform (black curve), for the Zn(Tb)S and Zn(Eu)S nanoparticle solutions in chloroform with 0.1% water (red curve), and for the Zn(Tb)S/Tb salt and Zn(Eu)S/Eu salt solutions in chloroform with 0.1% water (blue curve). For clarity, an enlarged part of the Eu^{3+} emission bands is shown in the inset of panel d. The excitation spectra for the Zn(Tb)S and Zn(Eu)S nanoparticles (black curve) were scaled to unity at the maximum intensity (~275 nm), and the other spectra are plotted with respect to it. The emission spectra were normalized to unity for the Zn(Tb)S and Zn(Eu)S nanoparticles at the peak of the broad, blue emission band (~420 nm); the red and blue curves were scaled with respect to the black curve in each panel. The spectra are corrected for optical density at the excitation wavelength.

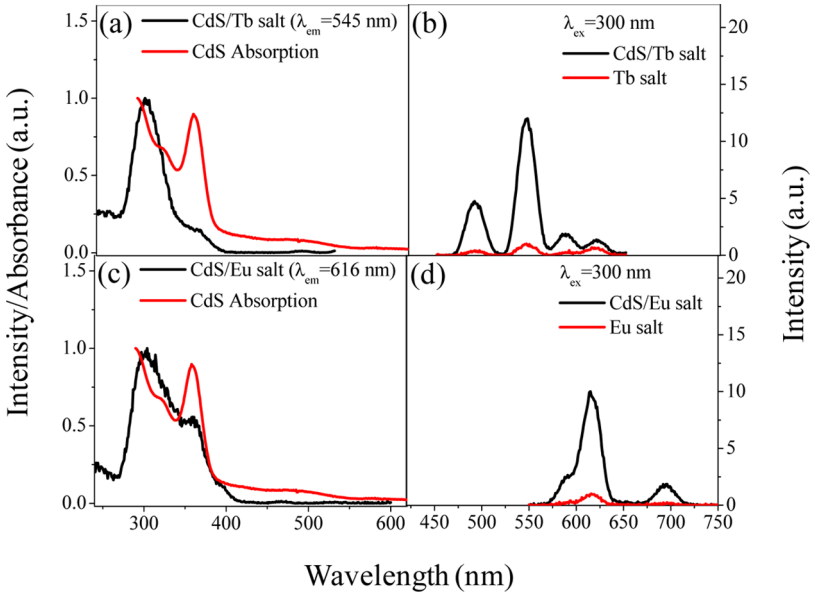

Figure 5. Time-gated normalized excitation and relative emission spectra of CdS/Tb salt and CdS/Eu salt systems are shown; the excitation spectra in panels a and c are compared to the absorption spectrum of the pure CdS nanoparticles. The samples were dissolved in toluene with an overall total lanthanide cation concentration of approximately 50 μM. The emission intensities in the presence of CdS nanoparticles were scaled with respect to the corresponding value in the absence of the nanoparticles, for which the emission intensity was normalized to unity at the band maximum.

conditions), and ZnS nanoparticles were added. The amount of ZnS nanoparticles in the solution was systematically varied and quantified by measuring the absorbance at 300 nm both before and after their addition. Figure 3b plots the change in the Eu^{3+} emission, scaled to the intensity without ZnS nanoparticles, as a function of the solution's absorbance change (ΔA) at 300 nm. These data reveal a correlation between the increase in the Eu^{3+} $^5D_0 \rightarrow {}^7F_2$ luminescence band centered at ~616 nm and the increase in absorbance at 300 nm (Figure 3, panel b). These data establish that the ZnS nanoparticles can increase the luminescence of Eu^{3+} ions by at least 60 times. Further control experiments are described in the Supporting Information (see Table S1). These findings show that the observed Eu^{3+} luminescence signal originates from a transfer of excitation energy from the ZnS nanoparticles to Eu^{3+}; i.e., ZnS nanoparticles act as an antenna for Eu^{3+} in these systems.

dx.doi.org/10.1021/jp404947x | J. Phys. Chem. C 2013, 117, 14451−14460

Luminescence Spectra for Zn(Ln)S Doped Nanoparticles in Ln Salt Solutions. *Zn(Tb)S/Tb Salt (Strategy I; 0.1% Water, See Materials and Methods Section).* Figure 4 (top panels) shows steady-state excitation and emission spectra of the Zn(Tb)S (black and red curves) and Zn(Tb)S/Tb salt (blue curve) solutions. As a control, the spectra of Zn(Tb)S nanoparticles were collected with ∼0.1% water added to the chloroform solution (red curve), and they reveal little effect of the water on the excitation and emission spectra. Table 1 reports the relative Tb^{3+} band centered quantum yields. The excitation spectra of the Zn(Tb)S (Figure 4a, λ_{em} = 545 nm, the Tb^{3+} centered emission) reveal a prominent feature at ∼275 nm, which is different from that of ZnS (see Figure 2 and Figure S3 left panel in the Supporting Information) and indicates a change in the ZnS electronic transition because of the Tb^{3+} ion incorporation. The emission spectra of Zn(Tb)S and Zn(Tb)S/Tb^{3+} (Figure 4b) show prominent Tb^{3+} bands like those shown in Figure 2b for ZnS/Tb^{3+}; see discussion of Figure 2b for band assignment.

Zn(Eu)S/Eu Salt (Strategy I, 0.1% Water, See Materials and Methods Section). Figure 4 (bottom panels) depicts steady-state excitation and emission spectra of the Zn(Eu)S (black and red curves) and the Zn(Eu)S/Eu salt (blue curve) solutions. Addition of 0.1% water to the Zn(Eu)S solution (red curve) results in some small changes in the spectra. The Zn(Eu)S/Eu^{3+} solutions show some increase in the Eu^{3+} emission over that observed for Zn(Eu)S solutions; however, the effect is less dramatic than in the case of Tb^{3+}. The excitation spectrum, obtained by monitoring the Eu^{3+} centered emission, reveals a prominent feature at ∼275 nm, which is different than that found for the ZnS and ZnS/Eu^{3+} salt solutions (see Figure 2c; also see Figure S3 (right panel)). This result is similar to that observed in the Zn(Tb)S/Tb salt system. The similarity of the excitation spectral changes for Zn(Eu)S and Zn(Tb)S suggests that it arises from changes in the ZnS electronic transition because of the creation of localized defects (Eu^{3+} and Tb^{3+} dopant sites).

Luminescence Spectra for CdS Nanoparticles in Ln Salt Solutions. The generality of the postsynthetic salt addition for sensitizing Ln^{3+} emission was tested by replacing the ZnS nanoparticles with CdS nanoparticles. CdS nanoparticles were chosen because of our previous work with Cd(Ln)S-doped nanoparticles and their luminescence sensitization efficiency.[31] Experiments were undertaken in which Tb(III) nitrate or Eu(III) nitrate were added separately to solutions of the commercially available oleic acid-capped CdS nanoparticles (see Figure 5). Note that the capping ligand for the CdS nanoparticles is different from that used in the synthesis of ZnS nanoparticles. A comparison of the observed Tb^{3+} (Eu^{3+}) luminescence intensities reveals an enhanced Tb^{3+} (Eu^{3+}) luminescence signal in the presence of CdS nanoparticles (black curves, Figure 5b,d), than for the Tb^{3+} (Eu^{3+}) in chloroform salt solutions (red curves, Figure 5b,d). The overlap of the Eu^{3+} $^5D_0 \rightarrow {}^7F_1$ transition at ∼590 nm and $^5D_0 \rightarrow {}^7F_2$ transition at ∼616 nm is caused by the wider slit widths, which were needed to acquire the weaker signals in these time-gated spectra (see Materials and Methods section). The excitation spectra (black curve), reveal two bands centered at around 300 and 360 nm. The 360 nm band in the excitation spectra coincides with the first exciton band of the CdS absorption spectrum (red curve), demonstrating that the CdS nanoparticles act as an antenna for sensitizing the Tb^{3+} and Eu^{3+} luminescence. In addition, the excitation spectrum for the CdS/Eu salt solutions display significant band intensities in the region of 300−360 nm, where no direct excitation of Eu^{3+} bands occurs (see Figure S4 in the Supporting Information). Both the Tb^{3+} and Eu^{3+} excitation spectra have a dominant peak in the 300 nm range, which demonstrates that higher energy photons are more efficient at sensitizing the lanthanide emission. Collectively, the measurements described above demonstrate that it is possible to sensitize the luminescence of Tb^{3+} and Eu^{3+} cations by the postsynthetic addition of the corresponding nitrate salts to solutions of the II−VI sulfide nanoparticles.

■ ASSESSING THE ROLE OF CORE VERSUS SURFACE SITES IN SENSITIZING Eu^{3+} LUMINESCENCE

The data and the analyses provided above do not allow for the determination of the lanthanide ions' location in the nanoparticle, i.e., in the bulk of the ZnS (or CdS) nanoparticle or near its surface. The determination of the precise location of dopant ions in a host nanoparticle lattice is a significant challenge, and few researchers have addressed this issue. Sarma and co-workers[55] have used a spectral shape analysis of luminescence bands to determine the location of dopant Mn^{2+} ions in CdS nanoparticles of different sizes. Other strategies for the identification of surface related species rely on the modification of dopant properties with changes in the surface ligand coating of the nanoparticles and/or the synthesis of core−shell materials. Van Veggel and co-workers[56] have explored these methods by analyzing how Eu^{3+} band intensities are altered in Eu^{3+} doped LaF_3 nanoparticles. Our work distinguishes surface localized lanthanide ions from core localized lanthanide ions by analyzing the excited state decay rate of the Eu^{3+} centered emission and the relative luminescence intensities of the Eu^{3+} bands, which are sensitive to the symmetry of the local coordination environment.

Asymmetry Ratio. Although the intraconfigurational 4f−4f lanthanide luminescence bands are shielded, several transitions are sensitive to the environment, and some of them are considered to be hypersensitive.[9] For Eu^{3+}, the $^5D_0 \rightarrow {}^7F_2$ transition (centered at ∼616 nm), which is of electric dipole character and is forbidden in a perfectly octahedral environment, becomes more allowed and has a higher oscillator strength in a less symmetric environment.[9] In contrast, the $^5D_0 \rightarrow {}^7F_1$ transition of the Eu^{3+} ion (centered at ∼590 nm) is an f−f magnetic dipole transition that is largely insensitive to the environment around the Eu^{3+} ion. Thus the intensity ratio of the $^5D_0 \rightarrow {}^7F_2$ transition to the $^5D_0 \rightarrow {}^7F_1$ transition is a parameter that can be used to gauge the asymmetry around the Eu^{3+} ions. The higher the value of this intensity ratio, the more asymmetric is the electronic environment around the Eu^{3+} ions. [The intensity ratio of the Eu^{3+} bands results from the spatial arrangement of coordinating units (ligands) and their electronic character (chemical nature).] By postulating that surface sites are more asymmetric than core sites, the intensity ratio can be used to assess the relative contribution of core and surface bound Eu^{3+} ions to the overall emission.

For this analysis, the asymmetry parameter AS is defined as

$$AS = \int I_{em}[{}^5D_0 \rightarrow {}^7F_2]\,d\nu \Big/ \int I_{em}[{}^5D_0 \rightarrow {}^7F_1]\,d\nu \qquad (1)$$

where the band intensities are integrated over frequency ν. The AS values are reported in Table 2, and the values in parentheses indicate the number of independent measurements. The error in the AS determination arises predominantly from the error in

dx.doi.org/10.1021/jp404947x | J. Phys. Chem. C 2013, 117, 14451−14460

Table 2. Asymmetry Parameter Values for Eu^{3+} in Different Systems Studied[a]

chloroform solutions	$\int I_{em}\ [^5D_0-^7F_2]\ d\nu / \int I_{em}\ [^5D_0-^7F_1]\ d\nu$
pure Eu salt	3.7 ± 0.2 (2)[a]
Zn(Eu)S	4.8 ± 0.1 (4)[a]
Zn(Eu)S[c]	4.6 ± 0.2 (4)[a]
ZnS/Eu salt[b,c]	5.5 ± 0.6 (5)[a]
Zn(Eu)S/Eu salt[b,c]	5.6 ± 0.1 (3)[a]

[a]The numbers in the parentheses indicate the number of independent measurements used to calculate the average and standard deviation values. [b]The europium(III) nitrate·xH_2O salt was used for the experiments. [c]Samples dissolved in chloroform with 0.1% water.

sample preparation and reflects the difficulty in adding a precise and reproducible amount of salt to the chloroform solutions.[57] For the systems investigated here, the postsynthesis addition of Eu^{3+} ions, either the ZnS/Eu^{3+} or Zn(Eu)S/Eu^{3+} nanoparticle solutions, causes an increase in the average asymmetry of the Eu^{3+} coordination environment, in comparison to the Zn(Eu)S system (a ratio of ~5.5 compared to one of ~4.6).

The data presented in the Table 2 display some clear trends. First, the addition of a small amount of water (~0.1% v/v) causes a small change in the asymmetry parameter for the Zn(Eu)S system; however, it still lies within the margin of error, and the dominant effect is a decrease in the overall quantum yield Φ_F (see Table 1). Second, the ZnS/Eu salt and Zn(Eu)S/Eu salt solutions have higher asymmetry ratios than the Zn(Eu)S solutions. The increase in the asymmetry parameter can be explained by postulating that more of the Eu^{3+} ions reside near (or on) the surface of the nanoparticles, and these coordination environments are more asymmetric. Third, the free Eu^{3+} in chloroform has the lowest asymmetry ratio among the different systems studied in the present work.

Luminescence Lifetime Measurements. A comparison between the luminescence decay curves obtained for the Tb^{3+} and Eu^{3+} salts in chloroform and those measured for the ZnS/Tb salt and ZnS/Eu salt solutions (strategy I, 0.1% water) reveals that the average emission lifetime of the Tb^{3+} and Eu^{3+} luminescence is greatly lengthened in the presence of ZnS (see Figure 6). The average lifetime obtained for the Tb^{3+} and Eu^{3+} salts in chloroform were found to be in the range of ~250 and ~125 microseconds, respectively, whereas the addition of ZnS nanoparticles caused a millisecond lifetime component to become apparent. The lifetime decay profiles for the nanoparticle solutions are well described by a biexponential decay law with a shorter lifetime component of ~500 μs (for both ZnS/Tb salt and ZnS/Eu salt) and a longer millisecond time scale component of 2.4 ms for ZnS/Tb salt and 1.5 ms for ZnS/Eu salt. Previous literature examples of luminescence lifetime values for well-protected Tb^{3+} and Eu^{3+} molecular complexes are 1.3 and 0.78 ms, respectively.[58] A comparison of the longer lifetime components obtained in the presence of nanoparticles with those from molecular complexes and ions in solution reveals that ZnS nanoparticles are better at protecting the Tb^{3+} and Eu^{3+} cations from nonradiative decay processes arising from the solvent.

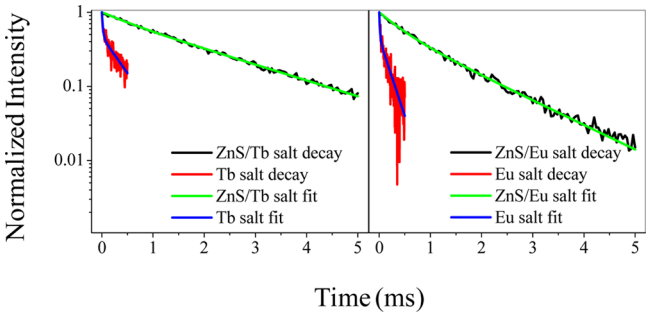

Figure 6. Examples of Tb^{3+} and Eu^{3+} band-centered luminescence decay traces and their fits by a double-exponential decay law are shown for solutions with and without ZnS nanoparticles. The adjusted R^2 values for the ZnS/Tb salt, Tb salt, ZnS/Eu salt, and Eu salt fits are 1.00, 0.90, 1.00, and 0.91, respectively. For pure lanthanide salts, the decays were acquired by dissolving them in chloroform. The ZnS/Tb and ZnS/Eu salt solutions were prepared in chloroform with 0.1% (v/v) water. Samples were excited at 354 nm and the emission was collected at 545 nm (Tb^{3+}) and 616 nm (Eu^{3+}).

The two different lifetime components could originate from two different environments in the ZnS nanoparticles; namely, the lanthanide ions in the core correspond to the millisecond time scale component and the lanthanide ions located near the ZnS surface correspond to the 500 μs component. In order to more clearly see the trend in the amplitudes of the lifetime components, the decay traces were best fit by fixing the lifetime components. Table 3 summarizes the lifetime decay parameters

Table 3. Luminescence Lifetime Parameters for Different Eu^{3+} Systems Studied[a,b]

system	a_1	τ_1 (ms)[c]	a_2	τ_2 (ms)[c]	$\langle\tau\rangle_{fix}$ (ms)
Zn(Eu)S	0.49 ± 0.03	0.5	0.51 ± 0.03	1.5	1.01
ZnS/Eu salt	0.54 ± 0.04	0.5	0.46 ± 0.04	1.5	0.96
Zn(Eu)S/Eu salt	0.59 ± 0.01	0.5	0.41 ± 0.01	1.5	0.91

[a]Samples were dissolved in chloroform with 0.1% water. [b]λ_{em} = 616 nm, Eu^{3+} $^5D_0 \rightarrow {}^7F_2$ transition. [c]Luminescence lifetime components were kept fixed in the fitting process.

of the Eu^{3+} band centered luminescence decays for the different cases, with lifetimes fixed at 500 μs and 1.5 ms. The average lifetime values for the fitting with fixed lifetime parameters were calculated according to eq 2:

$$\langle\tau\rangle_{fix} = a_1 \times 0.5\ \text{ms} + a_2 \times 1.5\ \text{ms} \quad (2)$$

The corresponding value calculated from freely varying all parameters in the fitting procedure were calculated according to eq 3,

$$\langle\tau\rangle_{vary} = \sum_i a_i\tau_i \quad (3)$$

The average difference between $\langle\tau\rangle_{vary}$ and $\langle\tau\rangle_{fix}$ lifetime values was found to be less than 2%. This comparison shows that the fitting by fixed lifetime parameters provides an acceptable parametrization of the decay profile. The Eu^{3+} lifetime parameters in Table 3 reveal that the amplitude of the short lifetime (0.5 ms) component in the ZnS/Eu salt and Zn(Eu)S/Eu salt is only higher by ~5−10% as compared to the Zn(Eu)S system.

In order to further characterize the Eu^{3+} band centered luminescence decays, the decay curves were fit by a distribution of lifetimes for the Zn(Eu)S and Zn(Eu)S/Eu salt solutions (see Figure 7). Comparison of the lifetime distribution shows that for the Zn(Eu)S/Eu salt solutions, the shorter lifetime components are more prevalent than for the Zn(Eu)S

dx.doi.org/10.1021/jp404947x | J. Phys. Chem. C 2013, 117, 14451−14460

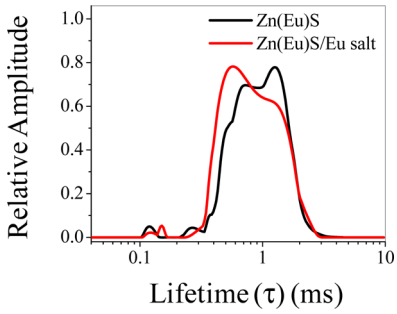

Figure 7. Luminescence lifetime distribution of the Zn(Eu)S and Zn(Eu)S/Eu salt systems studied. In each case, the area under the curve has been normalized to unity.

solutions. The increase in the amplitude of the shorter lifetime components in the Zn(Eu)S/Eu salt solutions is consistent with an enhancement of surface related Eu^{3+} population and corroborates the trend of an increased amplitude for the shorter lifetime component in the double-exponential decay fitting analysis (see Table 3).

CONCLUSION

This work presents and demonstrates a novel strategy to create Tb^{3+} and Eu^{3+} luminophores by postsynthetic, external addition of Tb^{3+} and Eu^{3+} salts to solutions of II–VI semiconductor nanoparticles (ZnS and CdS). The lanthanide luminescence in the externally added salt systems is demonstrated to be similar and of comparable intensity to the corresponding synthetically incorporated systems with the ZnS nanoparticles acting as an antenna.[31] Photophysical characterization, based on the analysis of the asymmetry ratio and the luminescence decay, reveals a small but discernible enhancement of the surface related contribution to the luminescence of the postsynthetically treated systems, as compared to the corresponding synthetically incorporated (doped) system. These data indicate that the distribution of lanthanide ions in the ZnS nanoparticles show a small preference for surface localized sites for the postsynthetic addition, as compared to the synthetically doped ZnS. Similar postsynthetic salt addition experiments with CdS nanoparticles reveal an increase in Tb^{3+} and Eu^{3+} luminescence in the presence of nanoparticles, as compared to the free salt case, suggesting that this approach is broadly applicable. The lanthanide luminescence sensitization that is found by postsynthetic salt addition offers a rapid and less synthetically demanding approach to sensitize the Tb^{3+} and Eu^{3+} luminescence, facilitating the scope of their applications.

MATERIALS AND METHODS

Chemicals. Trioctylphosphine [TOP] (90%), trioctylphosphine oxide [TOPO] (90%), zinc stearate (tech.), and octadecene (90% tech.) were purchased from Sigma-Aldrich-Fluka, St. Louis, MO. Tetracosane (99%) was purchased from Acros. Chloroform was purchased from J. T. Baker, Phillipsburg, NJ. Toluene was purchased from Fisher Scientific, Pittsburgh, PA. Sulfur was purchased from Fisher Scientific, Pittsburgh, PA. Terbium(III) nitrate (99.9%) was purchased from Strem and europium(III) nitrate (99.99%) was purchased from Aldrich. In all cases, hydrated lanthanide salts were used. *n*-Hexane and 1-octanol were purchased from Acros, and ethyl acetate was purchased from EMD, Gibbstown, NJ. Argon gas was purchased from Valley National, Pittsburgh, PA. All chemicals were used as purchased without additional purification.

ZnS-Based Nanoparticle Synthesis. All ZnS nanoparticle systems were synthesized using a noncoordinating solvent system consisting of octadecene and tetracosane. Zinc stearate and lanthanide nitrate salts were used as cation precursors, and elemental sulfur served as the anion precursor. Tetracosane (4.0 g), octadecene (3.0 mL), TOPO (1.7 g), and 0.68 mmol of zinc stearate were loaded into a three neck, round-bottom flask and refluxed at 300 °C while stirring under nitrogen. The lanthanide stock solution (0.12 mmol lanthanide nitrate dissolved in trioctylphosphine) was injected after approximately ∼2 h of heating and allowed to stir within the reaction mixture for 1 h. The sulfur stock solution (sulfur powder dissolved in 2.5 mL octadecene) was injected ∼1 h after the lanthanide stock solution injection. After 20 min of growth, the reaction was quenched by removal of the heat source and all of the reaction mixture was collected. The resulting nanoparticles were then redispersed in chloroform for spectroscopic analysis.

Pure (not incorporating lanthanides) ZnS nanoparticles were prepared using the methods described above; however, the zinc stearate precursor was increased to 0.80 mmol, and the lanthanide stock solution preparation was omitted. For purification of nanoparticles, solid raw material from the synthesis was dissolved in chloroform. To this solution, methanol was added dropwise until a precipitate formed. The precipitate was isolated by centrifugation and was used for TEM measurements.

CdS Nanoparticles. CdS nanoparticles with oleic acid as capping ligand, absorbance peak maximum of 360 nm, were purchased from NN Laboratories as a solution in toluene and were used as received.

Sample Preparation. To prepare the solutions for the external addition experiments with the ZnS nanoparticles, two different strategies were used. In strategy I, a known (maintaining the weight ratio of Ln^{3+} ions to the total weight of the synthesized nanoparticles) and quantitative amount of Ln^{3+} salt was added to the nanoparticle solution. The externally added salts were dissolved by adding a small amount of water (∼0.1% v/v). Incorporation of a small amount of polar solvent to dissolve the externally added salt is a well-known procedure described in the literature.[35] In strategy II, Eu^{3+} salt was sonicated in chloroform for approximately one week at ∼40–45 °C. The resulting suspension was filtered and an additional amount of chloroform was added to the filtrate to obtain a total volume of ∼3 mL. Synthesized ZnS nanoparticles were added to this solution. In this way, the solution contains a quantifiable (that is, the total amount of Eu^{3+} in the solution does not change before and after addition of ZnS nanoparticles) but uncertain amount of Eu^{3+} ions in the solution (the extremely low value of molar extinction coefficient of Eu^{3+} ions in chloroform prevented the determination of its exact amount by UV–vis absorption technique). Supplementary water was not added to these solution preparations of the solutions described under strategy II. It is to be noted that the exact amount of Eu^{3+} ions in these samples does not impact the conclusions in a significant way; as long as the total amount of Eu^{3+} ions remains fixed. This experiment reveals the role of ZnS nanoparticles for the sensitization of Eu^{3+} luminescence in these systems.

For performing experiments with CdS nanoparticles, a comparison was made between the respective lanthanide bands' luminescence in the presence and in the absence of

dx.doi.org/10.1021/jp404947x | J. Phys. Chem. C 2013, 117, 14451–14460

nanoparticles. The samples were dissolved in toluene. Lanthanide salts were introduced into the solutions from a methanol stock solution with 0.1% (v/v) methanol content.

Steady-State Optical Measurements. Steady-state absorption spectra were obtained with a Perkin-Elmer Lambda 9 or an Agilent 8453 UV−visible spectrophotometer. Steady-state excitation and emission spectra were recorded using either a Jobin Yvon Horiba Fluorolog-322 or a Jobin Yvon Horiba Fluoromax-3. No significant differences were observed by comparing results obtained from these two instruments. In all cases, spectra were corrected for excitation and emission response (lamp, detector, and monochromators). Time-gated spectra were collected in a Cary Eclipse fluorometer. A quartz 1-cm path length cuvette was used for all spectroscopic experiments. All measurements were performed at room temperature. Steady-state spectra were acquired with excitation and emission slits of 4 and 4 nm respectively. The steady-state spectra were acquired with long pass filters that eliminated the excitation light. For time-gated measurements, the spectra were acquired with excitation and emission slits of 20 and 20 nm respectively. For the acquisition of time-gated spectra, the filter arrangement was adjusted from the software by selecting the "Auto" option to eliminate the excitation light.

Quantum Yields. Absorption spectra were recorded on a Perkin-Elmer Lambda 9 spectrometer that was coupled to a personal computer using software supplied by Perkin-Elmer. Relative quantum yields were calculated by scaling the emission intensities to the value for the synthetically incorporated Zn(Ln)S system, whose quantum yield was set to unity. All spectra were corrected for the excitation and emission instrument responses. The quantum yield values were calculated using eq 4:

$$\frac{\Phi_x}{\Phi_r} = \frac{A_r(\lambda_r)\cdot I(\lambda_r)\cdot \eta_x^2 D_x}{A_x(\lambda_x)\cdot I(\lambda_x)\cdot \eta_r^2 D_r} \quad (4)$$

where the subscript r denotes the reference and x denotes the sample; A is the absorbance at the excitation wavelength (λ), I is the intensity of the excitation light, η is the refractive index (η = 1.446 in chloroform), and D is the measured integrated luminescence intensity. For the ZnS/Ln^{3+} systems studied, the lanthanide quantum yields were determined by integrating over the narrow Ln^{3+} emission bands, with the nanoparticle's broad band steady-state emission subtracted. The integration was performed over all the Tb^{3+} and Eu^{3+} luminescence bands that were visible in the steady-state mode.

Asymmetry Ratios. Asymmetry ratios for the Eu^{3+} ions were calculated by subtracting the nanoparticle's emission contribution from the total steady-state emission spectrum. Typically the region of interest in the spectrum was first interpolated with three data points to establish a baseline. This baseline was then plotted with a 1-nm resolution and subsequently subtracted from the acquired experimental spectrum. This process assumes that two adjacent Eu^{3+} bands are always separated by a zero baseline. Because of the presence of experimental noise, the subtraction process sometimes resulted in the generation of some small negative values. In such occurrences, the intensity was set to zero. The respective bands were integrated on the wavenumber scale and the ratios were then calculated.

Lifetime Measurements. Luminescence lifetime measurements on the Tb^{3+} and Eu^{3+} signals were performed by excitation of solutions in 1-cm quartz cuvettes using an Nd:YAG Continuum Powerlite 8100 laser (354 nm, third harmonic) as the excitation source. Emission was collected at a right angle to the excitation beam, and wavelengths were selected by a monochromator (Spectral Products CM 110). The signal was monitored using a Hamamatsu R928 photomultiplier tube, collecting the signal output with a 500 MHz bandpass digital oscilloscope (Tektronix TDS 620B). Signals from ∼2000 flashes were collected and averaged. Typically, all decay traces were collected with 2 ms/division of the oscilloscope. Luminescence lifetimes were averaged from multiple (at least three) measurements. Experimental luminescence decay curves were imported into Origin 8.0 and analyzed using the Advanced Fitting Tool. In all cases, the first 200 μs data points were systematically removed and the time axis was shifted to zero before fitting. This procedure removes any fast contribution in the decay trace that could originate from scattering of the excitation light or the nanosecond lived nanoparticle emission. However, this preliminary data treatment results in the loss of early time (<200 μs) information. Luminescence lifetime distributions were calculated using the Edinburgh's FAST decay analysis software. The distribution curves have been generated with 200 logarithmically spaced time points.

■ ASSOCIATED CONTENT

Supporting Information

Additional information as noted in text. This information is available free of charge via the Internet at http://pubs.acs.org.

■ AUTHOR INFORMATION

Corresponding Author

*(D.H.W.) Telephone: 1-412-624-8430; E-mail: dave@pitt.edu. (S.P.) Telephone: +33 238 255 652, E-mail: stephane.petoud@cnrs-orleans.fr.

Present Address

[§]Centre for Research in Nanoscience and Nanotechnology, University of Calcutta, JD-2, Sector-III, Saltlake City, Kolkata-700098, West Bengal, India.

Notes

The authors declare no competing financial interest.

■ ACKNOWLEDGMENTS

We acknowledge financial support from the National Institutes of Health via NIH Grant R21-EB008257-01A1. S.P. acknowledges support in France from la Ligue contre le Cancer and from Institut National de la Santé et de la Recherche Médicale (INSERM). P.M. and D.H.W. acknowledge support in part from the National Science Foundation (CHE 1057981). The work in France was carried out within the COST Action D38 and CM1006. We thank Dr. Susheng Tan of the Petersen Institute of Nanoscience and Engineering at the University of Pittsburgh for help with the HRTEM measurements.

■ REFERENCES

(1) Richardson, F. S. Terbium(III) and Europium(III) Ions as Luminescent Probes and Stains for Biomolecular Systems. *Chem. Rev.* **1982**, *82*, 541−552.

(2) Moore, E. G.; Samuel, A. P. S.; Raymond, K. N. From Antenna to Assay: Lessons Learned in Lanthanide Luminescence. *Acc. Chem. Res.* **2009**, *42*, 542−552.

(3) Hildebrandt, N.; Löhmannsröben, H.-G. Quantum Dot Nanocrystals and Supramolecular Lanthanide Complexes − Energy Transfer

Systems for Sensitive *In Vitro* Diagnostics and High Throughput Screening in Chemical Biology. *Curr. Chem. Biol.* **2007**, *1*, 167−186.
(4) Binnemans, K. Lanthanide-Based Luminescent Hybrid Materials. *Chem. Rev.* **2009**, *109*, 4283−4374.
(5) Montgomery, C. P.; Murray, B. S.; New, E. J.; Pal, R.; Parker, D. Cell-Penetrating Metal Complex Optical Probes: Targeted and Responsive Systems Based on Lanthanide Luminescence. *Acc. Chem. Res.* **2009**, *42*, 925−937.
(6) Bünzli, J.-C. G.; Piguet, C. Taking Advantage of Luminescent Lanthanide Ions. *Chem. Soc. Rev.* **2005**, *34*, 1048−1077.
(7) Eliseeva, S. V.; Bünzli, J.-C. G. Lanthanide Luminescence for Functional Materials and Bio-sciences. *Chem. Soc. Rev.* **2010**, *39*, 189−227.
(8) Bünzli, J.-C. G.; Eliseeva, S. V. Lanthanide NIR Luminescence for Telecommunications, Bioanalyses and Solar Energy Conversion. *J. Rare Earths* **2010**, *28*, 824−842.
(9) Bünzli, J.-C. G. Lanthanide Luminescence for Biomedical Analyses and Imaging. *Chem. Rev.* **2010**, *110*, 2729−2755.
(10) Thibon, A.; Pierre, V. C. Principles of Responsive Lanthanide-Based Luminescent Probes for Cellular Imaging. *Anal. Bioanal. Chem.* **2009**, *394*, 107−120.
(11) Nockemann, P.; Beurer, E.; Driesen, K.; Deun, R. V.; Hecke, K. V.; Meervelt, L. V.; Binnemans, K. Photostability of a Highly Luminescent Europium β-Diketonate Complex in Imidazolium Ionic Liquids. *Chem. Commun.* **2005**, 4354−4356.
(12) Carnall, W. T.; Fields, P. R. *Lanthanide/Actinide Chemistry*; American Chemical Society: Washington DC, 1967; Vol. *71*.
(13) Tsien, R. Y.; Ernst, L.; Waggoner, A. Fluorophores for Confocal Microscopy: Photophysics and Photochemistry. In *Handbook of Biological Confocal Microscopy*, 3rd ed.; Pawley, J. B., Ed.; SpringerScience+Business Media: New York, 2006.
(14) Waggoner, A. Fluorescent Labels for Proteomics and Genomics. *Curr. Opin. Chem. Biol.* **2006**, *10*, 62−66.
(15) Petoud, S. Novel Antennae for Luminescent Lanthanide Cations Emitting in the Visible and in the Near-Infrared: From Small Molecules to Polymetallic Lanthanide Containing Nanocrystals. *CHIMIA Int. J. Chem.* **2009**, *63*, 745−752.
(16) Uh, H.; Petoud, S. Novel Antennae for the Sensitization of near Infrared Luminescent Lanthanide Cations. *C. R. Chim.* **2010**, *13*, 668−680.
(17) Chengelis, D. A.; Yingling, A. M.; Badger, P. D.; Shade, C. M.; Petoud, S. Incorporating Lanthanide Cations with Cadmium Selenide Nanocrystals: A Strategy to Sensitize and Protect Tb(III). *J. Am. Chem. Soc.* **2005**, *127*, 16752−16753.
(18) Bhargava, R. N. Doped Nanocrystalline Materials - Physics and Applications. *J. Lumin.* **1996**, *70*, 85−94.
(19) Brennan, J. D.; Capretta, A.; Yong, K.; Gerritsma, D.; Flora, K. K.; Jones, A. Sensitization of Lanthanides by Nonnatural Amino Acids. *Photochem. Photobiol.* **2002**, *75*, 117−121.
(20) Kim, Y. H.; Baek, N. S.; Kim, H. K. Sensitized Emission of Luminescent Lanthanide Complexes Based on 4-Naphthalen-1-yl-Benzoic Acid Derivatives by a Charge-Transfer Process. *Chem. Phys. Chem.* **2006**, *7*, 213−221.
(21) Sato, S.; Wada, M. Relations between Intramolecular Energy Transfer Efficiencies and Triplet State Energies in Rare Earth β-Diketone Chelates. *Bull. Chem. Soc. Jpn.* **1970**, *43*, 1955−1962.
(22) Yang, C.; Fu, L.-M.; Wang, Y.; Zhang, J.-P.; Wong, W.-T.; Ai, X.-C.; Qiao, Y.-F.; Zou, B.-S.; Gui, L.-L. A Highly Luminescent Europium Complex Showing Visible-Light-Sensitized Red Emission: Direct Observation of the Singlet Pathway. *Angew. Chem., Int. Ed.* **2004**, *43*, 5010−5013.
(23) Chen, Y.; Lu, Z. Dye Sensitized Luminescent Europium Nanoparticles and Its Time-Resolved Fluorometric Assay for DNA. *Anal. Chim. Acta* **2007**, *587*, 180−186.
(24) Sivakumar, S.; van Veggel, F. C. J. M.; Raudsepp, M. Sensitized Emission from Lanthanide-Doped Nanoparticles Embedded in a Semiconductor Sol−Gel Thin Film. *Chem. Phys. Chem.* **2007**, *8*, 1677−1683.
(25) Chen, X.; Luo, W.; Liu, Y.; Liu, G. Recent Progress on Spectroscopy of Lanthanide Ions Incorporated in Semiconductor Nanocrystals. *J. Rare Earths* **2007**, *25*, 515−525.
(26) Anderson, W. W. Tb^{3+} as a Recombination Center in ZnS. *Phys. Rev.* **1964**, *136*, A556−A560.
(27) Palm, J.; Gan, F.; Zheng, B.; Michel, J.; Kimerling, L. C. Electroluminescence of Erbium-Doped Silicon. *Phys. Rev. B* **1996**, *54*, 17603−17615.
(28) Klik, M. A. J.; Gregorkiewicz, T.; Bradley, I. V.; Wells, J.-P. R. Optically Induced Deexcitation of Rare-Earth Ions in a Semiconductor Matrix. *Phys. Rev. Lett.* **2002**, *89*, 227401−1−227401−4.
(29) Planelles-Aragó, J.; Cordoncillo, E.; Ferreira, R. A. S.; Carlos, L. D.; Escribano, P. Synthesis, Characterization and Optical Studies on Lanthanide-Doped CdS Quantum Dots: New Insights on CdS → Lanthanide Energy Transfer Mechanisms. *J. Mater. Chem.* **2011**, *21*, 1162−1170.
(30) Beeby, A.; Clarkson, I. M.; Dickins, R. S.; Faulkner, S.; Parker, D.; Royle, L.; de Sousa, A. S.; Williams, J. A. G.; Woods, M. Non-Radiative Deactivation of the Excited States of Europium, Terbium and Ytterbium Complexes by Proximate Energy-Matched OH, NH, and CH oscillators: An Improved Luminescence Method for Establishing Solution Hydration States. *J. Chem. Soc., Perkin Trans. 2* **1999**, 493−503.
(31) Mukherjee, P.; Shade, C. M.; Yingling, A. M.; Lamont, D. N.; Waldeck, D. H.; Petoud, S. Lanthanide Sensitization in II−VI Semiconductor Materials: A Case Study with Terbium (III) and Europium (III) in Zinc Sulfide Nanoparticles. *J. Phys. Chem. A* **2011**, *115*, 4031−4041.
(32) White, K. A.; Chengelis, D. A.; Zeller, M.; Geib, S. J.; Szakos, J.; Petoud, S.; Rosi, N. L. Near-Infrared Emitting Ytterbium Metal−Organic Frameworks with Tunable Excitation Properties. *Chem. Commun.* **2009**, 4506−4508.
(33) Cross, J. P.; Lauz, M.; Badger, P. D.; Petoud, S. Polymetallic Lanthanide Complexes with PAMAM−Naphthalimide Dendritic Ligands: Luminescent Lanthanide Complexes Formed in Solution. *J. Am. Chem. Soc.* **2004**, *126*, 16278−16279.
(34) White, K. A.; Chengelis, D. A.; Gogick, K. A.; Stehman, J.; Rosi, N. L.; Petoud, S. Near-Infrared Luminescent Lanthanide MOF Barcodes. *J. Am. Chem. Soc.* **2009**, *131*, 18069−18071.
(35) Son, D. H.; Hughes, S. M.; Yin, Y.; Alivisatos, A. P. Cation Exchange Reactions in Ionic Nanocrystals. *Science* **2004**, *306*, 1009−1012.
(36) Mocatta, D.; Cohen, G.; Schattner, J.; Millo, O.; Rabani, E.; Banin, U. Heavily Doped Semiconductor Nanocrystal Quantum Dots. *Science* **2011**, *332*, 77−81.
(37) Sooklal, K.; Cullum, B. S.; Angel, S. M.; Murphy, C. J. Photophysical Properties of ZnS Nanoclusters with Spatially Localized Mn^{2+}. *J. Phys. Chem.* **1996**, *100*, 4551−4555.
(38) Dong, C.; van Veggel, F. C. J. M. Cation Exchange in Lanthanide Fluoride Nanoparticles. *ACS Nano* **2009**, *3*, 123−130.
(39) Chen, L.; Zhang, J.; Lu, S.; Ren, X.; Wang, X. On the Energy Transfer from Nanocrystalline ZnS to Tb^{3+} Ions Confined in Reverse Micelles. *Chem. Phys. Lett.* **2005**, *409*, 144−148.
(40) Robinson, R. D.; Sadtler, B.; Demchenko, D. O.; Erdonmez, C. K.; Wang, L.-W.; Alivisatos, A. P. Spontaneous Superlattice Formation in Nanorods Through Partial Cation Exchange. *Science* **2007**, *317*, 355−358.
(41) Sadtler, B.; Demchenko, D. O.; Zheng, H.; Hughes, S. M.; Merkle, M. G.; Dahmen, U.; Wang, L.-W.; Alivisatos, A. P. Selective Facet Reactivity during Cation Exchange in Cadmium Sulfide Nanorods. *J. Am. Chem. Soc.* **2009**, *131*, 5285−5293.
(42) Jing-hua, N.; Rui-nian, H.; Wen-lian, L.; Ming-tao, L.; Tian-zhi, Y. Electroluminescent Properties of a Device Based on Terbium-Doped ZnS Nanocrystals. *J. Phys. D: Appl. Phys.* **2006**, *39*, 2357−2360.
(43) Planelles-Aragó, J.; Julián-López, B.; Cordoncillo, E.; Escribano, P.; Pellé, F.; Viana, B.; Sanchez, C. Lanthanide Doped ZnS Quantum Dots Dispersed in Silica Glasses: An Easy One Pot Sol−Gel Synthesis for Obtaining Novel Photonic Materials. *J. Mater. Chem.* **2008**, *18*, 5193−5199.

(44) Ehrhart, G.; Capoen, B.; Robbe, O.; Beclin, F.; Boy, P.; Turrell, S.; Bouazaoui, M. Energy Transfer between Semiconductor Nanoparticles (ZnS or CdS) and Eu^{3+} Ions in Sol−Gel Derived ZrO_2 Thin Films. *Opt. Mater.* **2008**, *30*, 1595−1602.
(45) Dong, L.; Liu, Y.; Zhuo, Y.; Chu, Y. General Route to the Fabrication of ZnS and M-Doped (M = Cd^{2+}, Mn^{2+}, Co^{2+}, Ni^{2+}, and Eu^{3+}) ZnS Nanoclews and a Study of Their Properties. *Eur. J. Inorg. Chem.* **2010**, 2504−2513.
(46) Hou, S.; Yuen, Y.; Mao, H.; Wang, J.; Zhu, Z. Photoluminescence Properties of the Eu^{3+}-Doped ZnS Nanocrystals and the Crystal-Field Analysis. *J. Phys. D: Appl. Phys.* **2009**, *42*, 215105−5pp.
(47) Qu, S. C.; Zhou, W. H.; Liu, F. Q.; Chen, N. F.; Wang, Z. G.; Pan, H. Y.; Yu, D. P. Photoluminescence Properties of Eu^{3+}-Doped ZnS Nanocrystals Prepared in a Water/Methanol Solution. *Appl. Phys. Lett.* **2002**, *80*, 3605−3607.
(48) Sun, X. L.; Zhang, G. L.; Tang, G. Q.; Chen, W. J.; Hong, G. Y. The Site Symmetry of Eu^{3+} in ZnS:Eu Nanoparticle. *Chin. Chem. Lett.* **1999**, *10*, 807−810.
(49) Sun, L.; Yan, C.; Liu, C.; Liao, C.; Li, D.; Yu, J. Study of the Optical Properties of Eu^{3+}-Doped ZnS Nanocrystals. *J. Alloys Compd.* **1998**, *275*−*277*, 234−237.
(50) Wang, L.; Xu, X.; Yuan, X. Preparation and Photoluminescent Properties of Doped Nanoparticles of ZnS by Solid-State Reaction. *J. Lumin.* **2010**, *130*, 137−140.
(51) Yang, H.; Yu, L.; Shen, L.; Wang, L. Preparation and Luminescent Properties of Eu^{3+}-Doped Zinc Sulfide Nanocrystals. *Mater. Lett.* **2004**, *58*, 1172−1175.
(52) Brus, L. E. Electron−Electron and Electron−Hole Interactions in Small Semiconductor Crystallites: The Size Dependence of the Lowest Excited Electronic State. *J. Chem. Phys.* **1984**, *80*, 4403−4409.
(53) Li, L. S.; Pradhan, N.; Wang, Y.; Peng, X. High Quality ZnSe and ZnS Nanocrystals Formed by Activating Zinc Carboxylate Precursors. *Nano Lett.* **2004**, *4*, 2261−2264.
(54) One might argue that the observed increase in the Ln^{3+} luminescence intensity in Figure 3 results only from a concentration effect. Based on the following arguments, we, argue that this is not the case. (i) Although after sonication, some solid salt remains visible in the vial, experiments with salt in chloroform were performed after filtration. Therefore the filtrate was visibly clear, eliminating the possibility of the availability of an excess amount of salt available for ZnS to dissolve, and (ii) the nanoparticles used are hydrophobic, so there should not be any strong preference to dissolve the salts in the nanoparticles.
(55) Nag, A.; Cherian, R.; Mahadevan, P.; Gopal, A. V.; Hazarika, A.; Mohan, A.; Vengurlekar, A. S.; Sarma, D. D. Size-Dependent Tuning of Mn^{2+} d Emission in Mn^{2+}-Doped CdS Nanocrystals: Bulk vs Surface. *J. Phys. Chem. C* **2010**, *114*, 18323−18329.
(56) Sudarsan, V.; van Veggel, F. C. J. M.; Herring, R. A.; Raudsepp, M. Surface Eu^{3+} Ions Are Different than "Bulk" Eu^{3+} Ions in Crystalline Doped LaF_3 Nanoparticles. *J. Mater. Chem.* **2005**, *15*, 1332−1342.
(57) At this point, it is worth briefly summarizing the trend in asymmetry ratios that has been reported in the literature. By studying the Eu^{3+} luminescence with a wide range of ligands, van Veggel and coworkers[56] have reported an Eu^{3+} asymmetry ratio that ranges between 0.98 and 1.66. Selvan and coworkers (*J. Phys. Chem. B* **1999**, *103*, 7064−7067) have observed a 1.1 times increase in Eu^{3+} asymmetry ratio in gel systems with increasing Ag concentration. Deki and coworkers (*J. Phys. Chem. B* **2003**, *107*, 9161−9164) have found a 1.3 times increase in the asymmetry around the Eu^{3+} ions in their systems. Levy and coworkers (*Chem. Phys. Lett.* **1984**, *109*, 593−597) have found a 12 times increase in Eu^{3+} asymmetry on going from Eu/SiO_2 gel at 298 K to Eu/SiO_2 glass at 873 K. Except for a few reports, in general the Eu^{3+} asymmetry ratio values do not change drastically, which is probably at least qualitatively consistent with the core-like nature of the f electrons.
(58) Petoud, S.; Muller, G.; Moore, E. G.; Xu, J.; Sokolnicki, J.; Riehl, J. P.; Le, U. N.; Cohen, S. M.; Raymond, K. N. Brilliant Sm, Eu, Tb, and Dy Chiral Lanthanide Complexes with Strong Circularly Polarized Luminescence. *J. Am. Chem. Soc.* **2007**, *129*, 77−83.